

Training-Free Model Selection and Domain-Aware Score Calibration for First-Shot Anomalous Sound Detection

Grach Mkrtchian

Abstract—First-shot anomalous sound detection in DCASE Challenge Task 2 must flag anomalies of unseen machine types with a single threshold, without knowing whether a test clip comes from the data-rich *source* domain (990 normal training clips) or the data-scarce *target* domain (10). Two organizer-reported problems remain open: source- and target-domain AUC are negatively correlated across systems, and development-set performance does not predict evaluation-set performance. We address both with a training-free post-hoc layer over frozen audio embeddings: (i) per-domain quantile calibration shrunk toward a pooled map by a prior strength m , tracing a controllable source/target balance frontier, and (ii) a *label-free cross-validated domain-balance criterion* that ranks candidate configurations from training normals only, paired with a coarse development-labeled viability veto. On DCASE 2025, the criterion rank-predicts the official evaluation score across a 45-configuration grid (Spearman $\rho_s=+0.91$; family-block bootstrap 95% CI [+0.83, +0.95]) while development score is uninformative (+0.06, CI [-0.39, +0.31]). Criterion-based selection raises evaluation Ω from 55.83 to 59.34 (jackknife CI [2.2, 4.8]) and, on an extended grid, to 61.05—retrospectively fourth of 35 teams. Replication on DCASE 2023 and 2024 bounds the claim: development score is uninformative in all three years and well-balanced degenerate configurations recur (vetoed in every case), but under family-clustered uncertainty the criterion’s predictive evidence survives only in 2025; a fixed full-equalization default matches or beats criterion selection in both replication years, and the selection gain over development-based selection is significant only in 2025 (+5.2, jackknife CI [1.3, 9.2]). A DCASE 2026 forward test is frozen before the per-clip evaluation ground truth becomes available; all headline numbers are reproduced by the official evaluator.

Index Terms—Anomalous sound detection, machine condition monitoring, domain generalization, model selection, calibration, group-conditional quantile calibration, DCASE.

I. INTRODUCTION

MACHINE condition monitoring by sound must operate on machine types the developer has never recorded, be deployed with almost no data from the operating environment, and run at a fixed sensitivity chosen before any anomaly has been observed. DCASE Challenge Task 2 crystallizes this setting as *first-shot unsupervised ASD under domain generalization* [1], [2]: for each machine type, training data comprise 990 normal clips from a *source* domain and only 10 from a *target* domain; at test time the domain label is withheld, so anomalies from both domains must be separated from normal sounds with a *single* threshold, and the evaluation

machine types are disjoint from the development (henceforth “dev”) ones, forbidding per-machine tuning.

The 2025 organizers document two failure modes that remain open [1]. First, *source/target imbalance*: across the top twenty teams, source- and target-domain AUC are negatively correlated, and only four teams beat the official baselines in both domains simultaneously. Second, *dev→evaluation non-transfer*: “achieving high AUC values in the development dataset does not indicate high AUC in the evaluation dataset”—model selection on the dev set is unreliable.

This article argues that both failure modes are, at their core, calibration and model-selection problems, and that they can be attacked *post hoc*, on top of any frozen embedding extractor and any training-free anomaly-score backend, at negligible computational cost. The raw anomaly scores of source- and target-domain normal clips live on different scales, so no single threshold can be well placed for both; and the dev set is the wrong yardstick for choosing how strongly to correct this mismatch.

Our proposal, DACO (from *Domain-Aware Calibration*), has two parts whose importance our experiments rank in this order:

A *label-free selection criterion* (section IV-D). For any candidate configuration, repeatedly hold out half of each domain’s training normals, refit the score pipeline, and measure the Kolmogorov–Smirnov (KS) distance between the calibrated held-out source and target score distributions. The criterion measures how domain-balanced the configuration’s operating point is, uses no anomalies and no test data, and is therefore available for unseen machines at deployment. It is family-agnostic: it selects among raw, normalized, and calibrated scoring pipelines alike.

A *per-domain calibration layer with a controllable strength* (section IV). Test clips receive soft latent-domain weights from embedding-space proximity to the source and target training banks; the base score is mapped through per-domain quantile maps built from leave-one-out training scores; each map is shrunk toward the pooled map by a prior strength m , tracing a smooth frontier between the raw ranking ($m\rightarrow\infty$) and full per-domain equalization ($m=0$). The frontier turns “how strongly to calibrate” into a selectable quantity—the object the criterion selects.

Our main findings on DCASE 2025 Task 2 are:

- 1) *Dev and evaluation scores disagree structurally* (section VI-C): across a 45-configuration grid, dev Ω (the official harmonic-mean metric) increases with m (Spear-

G. Mkrtchian is an independent researcher (e-mail: g.mkrtchyan.m@gmail.com).

man $\rho_s=+0.45$) while evaluation Ω decreases (-0.96); their overall rank correlation is $+0.06$. This is a sharper, mechanism-level restatement of the organizers’ transfer observation.

- 2) *The label-free criterion transfers* (section VI-C): computed on dev machines, it rank-predicts evaluation Ω at $\rho_s=+0.91$ (family-block bootstrap 95% CI $[+0.83, +0.95]$; machine-level bootstrap $[+0.24, +0.97]$). Guarded selection by the criterion instead of dev Ω raises evaluation Ω from 55.83 (below the official Selective-Mahalanobis baseline; rank 23 when inserted into the 35-team leaderboard) to 61.05 (rank 4; extended grid, section VI-E)—with the identical training-free system pool.
- 3) *The calibration frontier controls the aggregate source/target trade-off* (section VI-B): the signed mean gap moves from $+13.8$ points (raw) to -1.2 ($m=0$, a slight target overshoot). We disclose that per-machine balance is a different story (mean absolute gap moves only from 15.1 to 14.0), and analyze the failure cases.
- 4) *The pattern is robust where it must be, and we map where it is not* (sections VI-D to VI-F): on three frozen backbones the criterion predicts evaluation rank at $\rho_s=+0.67$ to $+0.81$ while dev Ω swings between -0.03 and $+0.84$. Local-density score normalization [3] is itself strong on evaluation (61.04) but *rejected* by dev-based selection (56.5 dev vs. 58.7 raw); the criterion selects into that family. Replicating the full pipeline on DCASE 2023 and 2024 turns the single dev \rightarrow eval pair into three: dev Ω is uninformative in every year, well-balanced degenerate configurations recur in every year (the unguarded criterion selects one in three of five year-backbone settings; the veto catches all of them), and the criterion’s raw rank correlations are $+0.54$, -0.10 , and $+0.81$ (like-for-like 51-configuration grids)—but only the 2025 evidence survives family-clustered uncertainty analysis (section VI-F), so we claim criterion transfer for one year of three and treat 2023 as suggestive at most.
- 5) *A genuinely prospective test is pre-registered* (section VI-F): the DCASE 2026 evaluation data do not yet exist, so we froze the criterion-selected configuration on the released 2026 development set—selection, veto, channel policy, and artifact hashes committed to the public repository—before any outcome can be known.
- 6) *Everything is training-free and cheap* (section VI-G): embedding extraction runs once (1.9–9.4 ms/clip); a full configuration cycle on cached embeddings, criterion included, takes ~ 0.15 s per machine.

We also contribute a negative-result analysis: pure per-domain calibration ($m=0$) *harms* the dev set on specific machine geometries, the criterion does not predict *dev* performance, a purely label-free criterion can be gamed by degenerate score maps—which motivates the coarse dev-side viability veto we pair it with—and in two of three challenge years a fixed full-equalization default matches or beats criterion-based selection, concentrating the criterion’s demonstrated added

value in a single year. That the same calibration knob helps evaluation machines and hurts dev machines *is* the organizers’ transfer phenomenon; we show it can be navigated with deployment-legal signals, and we bound where the navigation helps.

II. RELATED WORK

A. Systems for domain-generalized ASD

The dominant DCASE Task 2 recipe learns discriminative embeddings with angular-margin auxiliary classification: sub-cluster AdaCos [4], self-supervised FeatEx [5], and subspace-projection AdaProj [6]; see the recent review of DCASE-related domain-shift work [7] for a taxonomy. Frozen audio foundation models (BEATs [8], EAT [9], PANNs [10]) with training-free backends are competitive: GenRep [11]—frozen BEATs + kNN with source/target memory banks, target-bank augmentation, and domain score normalization—placed second among teams in DCASE 2025 Task 2, and a recent systematic study finds the scoring backend matters more than pooling [12]. Our layer operates on top of exactly this system class. The official Selective-Mahalanobis baseline likewise keeps per-domain statistics [1]; per-domain *modeling* is standard—what is new here is pinning both domains’ normal scores to a common quantile scale and treating the strength of that correction as a selectable quantity.

B. Score normalization

The closest prior line is score normalization for domain generalization: ratio- and difference-based rescaling by local density of the reference set [13], [3], with a cluster-exit extension [14]. Normalization makes scores *comparable* across acoustic regions; per-domain quantile calibration additionally anchors them to an *operating point* (approximate per-domain false-positive rate, empirically validated in section VI-B). More importantly, that line does not treat dev \rightarrow eval transfer or model selection, which our experiments show is where the larger gain lies; indeed, dev-based selection would reject local-density normalization itself (section VI-E).

C. Conformal and group-conditional calibration

Conformal anomaly detection yields distribution-free p -values from calibration scores [15], [16], [17]. Our Stage-2 maps are Mondrian (group-conditional) in spirit [15], with the domain as the taxonomy; borrowing strength between small groups and a pooled calibration set connects to class-conditional conformal prediction with many classes [18] and conditional-guarantee work [19]. Recent applications to industrial and time-series monitoring include adaptive conformal detection on frozen time-series foundation models [20], weighted conformal p -values in low-data regimes [21]—whose granularity analysis directly bears on our 10-clip target domain—and conformal false-alarm control for cyber-physical systems [22]. Set-valued prediction pursues per-domain criteria for supervised domain generalization [23]. Weighting calibration data by proximity to the test point is itself an established idea—localized conformal prediction [24] and randomly-localized

weighting with robust guarantees [25]—so our soft latent-group membership should be read as a two-group special case of that principle rather than a new mechanism; likewise, the shrinkage form of eq. (2) is the classical m -estimate / partial-pooling estimator [26], [27] applied to quantile maps, and differs from the weighted-conformal construction of [21] in mixing *maps* rather than reweighting calibration points. We are not aware of prior work applying per-domain FPR anchoring of this kind to ASD; the method-level contribution is treating the pooling strength m as a selection axis—the frontier—rather than any single ingredient.

D. Label-free model selection for anomaly detection

Selecting anomaly detectors without labels is an open problem with its own literature: meta-learning from prior labeled collections (MetaOD [28]) and surrogate-signal ranking for time-series AD ([29]). In ASD specifically, [12] report a *failed* pseudo-validation selection experiment, underscoring the gap. A parallel lineage exists for unsupervised *domain adaptation*, where models must likewise be chosen without target labels: importance-weighted cross-validation [30], Deep Embedded Validation [31], and soft neighborhood density [32] construct label-free surrogates of target risk for classifiers. Our criterion differs in target and signal: it selects for *domain balance of the operating point* of an anomaly detector in the first-shot single-threshold setting, using only the machine’s own normal training audio, and is validated by dev→eval transfer against the official protocol. To our knowledge no prior work proposes a label-free selection signal for this specific setting—operating-point balance under first-shot domain generalization—though the surrogate-validation idea itself is well established.

III. PROBLEM SETTING

A. Data and protocol

We use DCASE 2025 Challenge Task 2 [1]. The dev set contains seven machine types (fan, gearbox, bearing, slider, valve, ToyCar, ToyTrain); the evaluation set contains eight novel types (AutoTrash, BandSealer, CoffeeGrinder, HomeCamera, Polisher, ScrewFeeder, ToyPet, ToyRCCar). Per machine type: 990 source-domain and 10 target-domain normal training clips (domain labels available for training data), and 200 test clips (100 normal, 100 anomalous; both domains) whose domain and condition are withheld at inference. All audio is single-channel 16 kHz, built from ToyADMOS2 [33] and MIMII DG [34]. Post-challenge ground truth for the evaluation set is published in the official evaluator repository, enabling offline scoring; we use it strictly for metric computation, never for selection.

B. Metrics

Following the official protocol, $AUC_{j,d}$ is computed per machine j and domain $d \in \{s, t\}$ using the normal test clips of domain d against *all* anomalous clips of both domains; $pAUC_j$ is the standardized partial AUC over the false-positive range

$[0, 0.1]$ over all test clips; the official score is the harmonic mean over machines and quantities,

$$\Omega = \mathcal{H}(\{AUC_{j,s}, AUC_{j,t}, pAUC_j\}_{j \in \mathcal{M}}), \quad (1)$$

reported $\times 100$ throughout. The harmonic mean punishes imbalance, which is why the source/target trade-off is damaging. Our implementation of eq. (1) matches the official evaluator: a 2000-trial randomized differential test against the evaluator’s per-domain filtering logic agrees to machine precision (script in the released code), and all headline evaluation-set numbers were additionally reproduced end-to-end by running the official evaluator on exported per-clip scores (section VI-C).

IV. METHOD

DACO operates after a frozen embedding extractor $\phi : \mathcal{X} \rightarrow \mathbb{R}^D$ and a base anomaly scorer A ; neither is modified. Let $\mathcal{B} = \{\phi(x_i)\}_{i=1}^N$ be a machine’s normal training embeddings ($N=1000$), partitioned by the known training-domain labels into \mathcal{B}_s ($n_s=990$) and \mathcal{B}_t ($n_t=10$).

A. Preliminaries: base scores and calibration scores

We use the k -nearest-neighbor cosine distance as the base score, $A(x) = \frac{1}{k} \sum_{z \in \text{NN}_k(x; \mathcal{B})} d_c(\phi(x), z)$, with d_c the cosine distance on ℓ_2 -normalized embeddings. Calibration scores for training clips are computed *leave-one-out* (LOO): the score of $x_i \in \mathcal{B}$ is its mean distance to its k nearest neighbors in $\mathcal{B} \setminus \{x_i\}$, mirroring test-time scoring while excluding the trivial self-match.

B. Stage 1: latent-domain assignment

The test-clip domain is unknown. Let $d_s(x) = \min_{z \in \mathcal{B}_s} d_c(\phi(x), z)$ and analogously $d_t(x)$. Soft weights are a softmax over $-d_g(x)/T$, $g \in \{s, t\}$, with temperature T set to the median of the machine’s pooled LOO calibration scores (the typical neighbor-distance scale); a hard variant uses $w_t = \mathbf{1}[d_t < d_s]$. Stage 1 uses only the machine’s own training data, respecting the first-shot constraint.

C. Stage 2: per-domain quantile calibration with shrinkage

For each domain g , let \hat{c}_g be the *interpolated* empirical CDF of the LOO calibration scores of \mathcal{B}_g : order statistics at plotting positions $i/(n_g+1)$, linearly interpolated, with a monotone rational right tail $q_{\max} + (1 - q_{\max})\xi/(\xi + \lambda)$, where $q_{\max} = n_g/(n_g+1)$, ξ is the exceedance over the largest calibration score s_{\max} , and $\lambda = \max(s_{\max} - \text{med}, 10^{-9})$ with med the median calibration score—so extreme scores retain their raw ordering rather than saturating; below the smallest calibration score the map interpolates linearly toward zero at score 0. Interpolation avoids the $1/(n_t+1)$ -granularity ties a step CDF would produce with $n_t=10$ [21].

Because ten points cannot support extreme quantiles, each domain map is shrunk toward the pooled map \hat{c}_{pool} (all N LOO scores) with prior strength $m \geq 0$:

$$c_g(a) = \frac{n_g \hat{c}_g(a) + m \hat{c}_{\text{pool}}(a)}{n_g + m}. \quad (2)$$

The calibrated score is $\tilde{A}(x) = \sum_g w_g(x) c_g(A(x))$.

What is and is not guaranteed. At $m=0$ each domain’s normal scores map approximately to $U(0,1)$, so one global threshold τ corresponds to a similar normal-exceedance rate $1-\tau$ in every latent domain. We deliberately call this *approximate* FPR equalization rather than a conformal guarantee: the LOO construction is jackknife-style rather than split-conformal (calibration scores are mutually dependent), linear interpolation forgoes the exactness of step-function conformal p -values, soft assignment mixes the two maps, any Stage-1 error breaks per-domain exchangeability, and for $m>0$ no guarantee is intended. The map also has data support only down to exceedance $1/(n_g+1)$; with $n_t=10$, all of the pAUC integration range except the sliver $[1/11, 1/10]$ lies in the extrapolated tail. We therefore validate the property empirically: at matched label-free thresholds, calibration roughly halves the cross-domain FPR imbalance relative to raw scoring (section VI-B). As $m \rightarrow \infty$ both maps coincide with \hat{c}_{pool} , a single monotone transform preserving the raw ranking; m thus *parametrizes the source/target balance frontier* (Fig. 1), turning calibration strength into a model-selection problem.

D. Stage 3: the selection criterion

Dev-set Ω is the standard selection signal, but it does not transfer (section VI-C). We select among configurations (here: m, k , assignment, calibration variant, score family) with a criterion computable from *training normals only*. For each of S random splits (indexed r), hold out half of each domain’s training normals, refit the pipeline (Preliminaries–Stage 2) on the remainder, push the held-out normals through it, and compute

$$C = \frac{1}{S} \sum_{r=1}^S \text{KS}(\tilde{A}(\mathcal{D}_s^r), \tilde{A}(\mathcal{D}_t^r)), \quad (3)$$

where \mathcal{D}_g^r is the held-out half of domain g in split r . Equation (3) is computed per machine; for fixed-configuration selection we aggregate as the mean over the dev machines, $C(\gamma) = |\mathcal{M}_{\text{dev}}|^{-1} \sum_j C_j(\gamma)$, while per-machine selection uses the target machine’s own C_j . Small C means the two domains’ normal score distributions nearly coincide, so one global threshold produces similar false-positive rates in both—the domain-balanced operating point that the harmonic-mean metric rewards. The criterion is defined for every configuration including the uncalibrated baseline, and uses no anomalies, no test clips, and no cross-machine statistics. We use $S=10$ with a fixed seed pairing splits across configurations; the selected configuration is unchanged for $S \in \{5, 10, 20\}$. Note the finite-sample floor: with only 5 held-out target clips per split, the two-sample KS statistic under identical distributions averages ≈ 0.36 per machine (± 0.012 for a 7-machine mean), so observed values (0.49–0.72) must be read relative to that floor, and differences of $\lesssim 0.01$ between configurations are noise—the criterion is a coarse region selector, not a fine ranker (section VI-C). One further subtlety: during criterion CV the pipeline is refit on half-size banks ($n'_g = n_g/2$, so $n'_t=5$), which makes the effective pooled weight in eq. (2) $m/(n'_g+m)$ at selection time versus $m/(n_g+m)$ at deployment—slightly

Algorithm 1 DACO scoring and configuration selection

Require: candidate configurations Γ ; per machine: training normals $\mathcal{B} = \mathcal{B}_s \cup \mathcal{B}_t$; labeled dev machines
Scoring (per machine, per configuration $\gamma \in \Gamma$):
1: compute the configuration’s training-bank calibration scores (LOO)
2: construct γ ’s score transform: per-domain quantile maps with shrinkage m (2), per-domain z -score or median-ratio, LDN, or the identity (raw)
3: score a test clip x by applying the transform, $\tilde{A}(x) = \sum_g w_g(x) c_g(A(x))$ for per-domain maps with soft or hard weights w_g
Selection:
4: **for** $\gamma \in \Gamma$ **do**
5: $C(\gamma) \leftarrow$ CV domain-balance criterion on training normals (3)
6: **end for**
7: $\mathcal{V} \leftarrow \Gamma$ without its bottom decile by dev Ω (veto)
8: **return** $\arg \min_{\gamma \in \mathcal{V}} C(\gamma)$

stronger shrinkage during selection. At $m=0$, where all headline picks lie, the two coincide; for $m>0$ the mismatch could be removed by rescaling $m' = m n'_g/n_g$, which we note as a limitation rather than adopt.

E. Viability veto

Balance is necessary but not sufficient: a degenerate score map can be perfectly balanced and detect nothing, and a label-free criterion cannot see detection power (a concrete example arises in section VI-E). Dev Ω , although unreliable for fine ranking, is reliable at flagging broken configurations: the degenerate maps in our grids fall 8–16 points below the dev-best. The full selection rule (algorithm 1) is therefore: *exclude the bottom decile of configurations by dev Ω , then minimize the criterion*. A threshold form of the veto (within δ of the dev-best) gives identical selections for $\delta \in [3, 8]$ on two of three backbones; we disclose the exceptions, and the veto’s origin, in section VI-D. The veto uses labeled dev data only—legal before any evaluation data exist. The complete rule is thus label-free *on the deployment machines*; dev labels enter only as a coarse veto, never as a ranking signal.

V. EXPERIMENTAL SETUP

Systems. Frozen backbones: BEATs iter3+ AS2M [8] (primary; time-mean-pooled frame features, 768-d), EAT-base [9] (CLS utterance token, 768-d; checkpoint `worstchan/EAT-base_epoch30_pretrain`), and PANNs CNN14-16k [10] (penultimate embedding, 2048-d; checkpoint `Cnn14_16k_mAP=0.438`). Base scorer: kNN cosine distance, $k \in \{1, 2, 4\}$. Configuration grid: raw; per-domain quantile calibration (eq. (2)) with $m \in \{0, 10, 30, 100, 300\} \times$ assignment {soft, hard}; per-domain z -score (the normalization family used by GenRep [11]); per-domain median-ratio; and the local-density normalization family (ratio/difference, density neighborhood $K \in \{1, 16\}$ [13], [3], reimplemented from the published

equations—the AGPL reference implementation was not consulted) plus calibration stacked on it. In total 45 configurations for the transfer study and 51 per backbone for the ablations.

Experiments. E1 reproduces baselines; E2 maps the balance frontier (dev set); E3 is the transfer and selection study; E4 repeats it across backbones; E5 is the head-to-head with local-density normalization; E6 reports cost; E7 replicates the full pipeline on DCASE 2023 and 2024 (datasets and post-challenge ground truth from the respective official Zenodo records and evaluator repositories) and pre-registers the DCASE 2026 forward test. The criterion uses $S=10$ splits, seed 0 (stability over seeds 0–9 reported); all other components are deterministic.

Hygiene. All selection signals are computed from training normals plus (for the veto only) labeled dev data. By construction, test labels and domains of the evaluation machines enter only the metric module and one explicitly-labeled oracle diagnostic; this can be verified directly in the released code, whose data loaders inject ground truth exclusively into test clips and whose selection paths consume training embeddings alone. The metric implementation passes a released 2000-trial randomized differential test against the official evaluator’s per-domain filtering logic (maximum absolute deviation 0), and headline results were re-scored end-to-end by the official evaluator on exported per-clip scores—which we release for every configuration appearing in a table, together with a configuration manifest, checkpoint SHA-256 pins, the environment lock, and scripts for every statistic in this paper, including the bootstrap and permutation procedures.

VI. RESULTS

A. Baseline reproduction (E1)

BEATs + kNN ($k=1$) attains dev $\Omega = 58.73$ versus 56.26 (Simple AE) and 55.34 (Selective Mahalanobis) for the official baselines (dev-set aggregates recomputed as harmonic means of the organizers’ published per-machine values); our frozen-embedding Selective-Mahalanobis and GMM backends reach 55.83 and 52.03, supporting kNN as the base scorer. The raw source/target gap is large (mean AUC_s 70.8 vs. AUC_t 57.0), reproducing the imbalance the protocol is designed to expose.

B. The balance frontier (E2)

Fig. 1 shows mean source vs. target AUC as m sweeps from 0 to 300. The *signed mean* gap moves smoothly from +13.8 points (raw) through -1.2 at $m=0$ (a slight target overshoot, visible above the diagonal in Fig. 1); the median per-machine gap drops from 15.2 to 3.6. Aggregate balance is thus controllable. Per-machine balance is not the same thing: the mean *absolute* gap only moves from 15.1 to 14.0, dominated by one machine (ToyCar) where calibration overshoots violently (source 75.8 \rightarrow 35.2, target 59.0 \rightarrow 84.5).

The mechanism of that failure is diagnostic (released as `diagnostics.csv`): on ToyCar only 6% of anomalies exceed the largest of the ten target LOO calibration scores while 99% exceed the source 90th percentile, so target-assigned

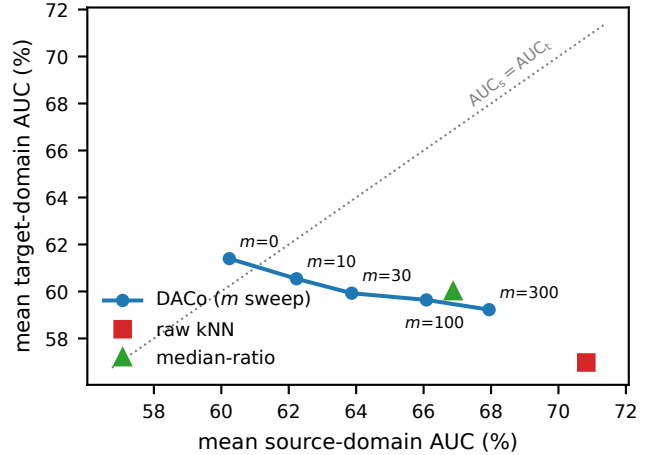


Fig. 1. The source/target balance frontier: mean source vs. target AUC over the seven dev machines (BEATs backbone; soft assignment, $k=1$). The prior strength m (eq. (2)) interpolates between the raw kNN ranking and full per-domain equalization; the dotted line marks $AUC_s=AUC_t$; the median-ratio variant sits near the frontier.

anomalies are pulled below mid-ranked source normals—even with oracle domain assignment. On the dev set, gains and losses follow Stage-1 assignment accuracy (measured on test normals; also released): fan (100%) gains +8.5 target-AUC points at $m=0$, ToyCar (85%) gains +25.5 on target while collapsing on source, and chance-level machines (bearing/slider/valve, 51–54%) are unaffected. We caution that this clean structure–response picture is a *dev-set observation*: across all 15 machines the rank correlation between train-side domain separability and target-AUC gain is only +0.39 ($p=0.15$), with low-separability gainers (ToyPet +16.0 at 0.55; AutoTrash +17.5 at 0.65) and one separable loser (ToyTrain -8.4 at 0.80); see Fig. 2. Dev Ω consequently does *not* improve along the frontier (raw 58.73; $m=0$: 56.29)—which is precisely why calibration strength must be selected, not fixed.

Finally, the operating-point property itself: at matched label-free global thresholds (nominal levels 0.1–0.5), calibration approximately halves the mean per-machine cross-domain FPR imbalance relative to raw scoring when averaged over all 15 machines ($|FPR_s - FPR_t|$ 0.16 vs. 0.31 at the 0.1 level; on the seven dev machines alone the imbalance instead increases, driven by ToyCar), although absolute FPR levels exceed nominal under the train \rightarrow test session shift (≈ 0.21 at nominal 0.10)—the approximate-equalization framing of section IV-C, validated and bounded.

C. Transfer and label-free selection (E3)

Fig. 3 is the central result. Across the 45-configuration grid, dev Ω carries no rank information about evaluation Ω ($\rho_s=+0.06$, family-block bootstrap 95% CI $[-0.39, +0.31]$, panel a); the label-free criterion computed on dev machines predicts it at $\rho_s=+0.91$ (panel b). The disconnect is structural, not noise: dev and evaluation Ω respond to the calibration-strength knob in opposite directions (ρ_s with $\log m$: +0.45

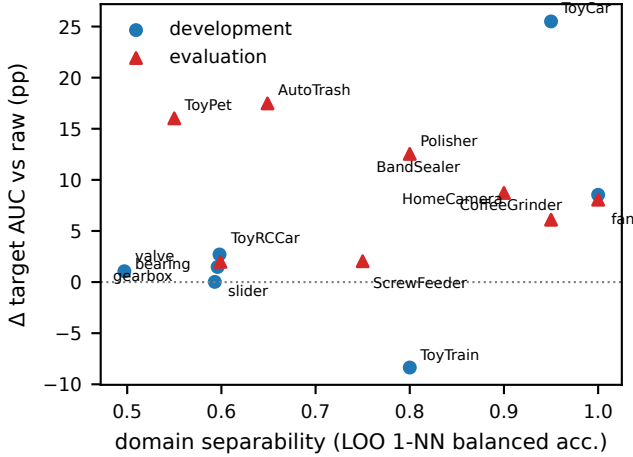


Fig. 2. Per-machine target-AUC gain of calibration ($m=0$, soft assignment, $k=1$, BEATs) over raw kNN ($k=1$) versus domain separability of the training normals (LOO 1-NN balanced accuracy). Circles: dev machines; triangles: evaluation machines (post-challenge ground truth used for metric computation only). The structure–response relationship is clean on dev but weak overall ($\rho_s=+0.39$, $p=0.15$): ToyPet and AutoTrash gain at low separability, ToyTrain loses at high separability.

vs. -0.96 ; within the conformal-soft family the dev–eval rank correlation is -0.79). The dev range is also compressed (3.1 vs. 5.2 points), so dev selection is noise-limited on top of being directionally wrong.

Because the 45 configurations cluster into seven method families (raw and the soft/hard variants of conformal, median-ratio, and z -score, each family pooling k and, for conformal, m), we report clustered uncertainty computed by released scripts: a family-block bootstrap (resampling the seven families, 5000 draws) gives a 95% CI of $[+0.83, +0.95]$; the rank correlation of the seven family means is $+0.93$ (exact permutation test over all $7!$ orderings: one-sided $p=0.0034$, two-sided $p=0.0067$); a machine-level bootstrap (resampling the 7 dev machines for the criterion and the 8 evaluation machines for Ω) is much wider, $[+0.24, +0.97]$, reflecting the small machine sets. The correlation survives family-structure stress tests: conformal-only $+0.89$, leave-one-family-out $+0.90$ to $+0.92$, dropping all conformal configurations $+0.92$. On the extended 51-configuration grid (adding the LDN family) the same correlation is $+0.81$ with family-block CI $[+0.43, +0.93]$ —the grid used for all cross-year comparisons below.

Is the correlation just re-reading m ? Within conformal families the criterion is close to monotone in m by construction, so we deconfound explicitly: partialling out $\log(m+1)$ and family membership across the full grid leaves a residual association of $+0.71$ (partial Spearman, $p<10^{-6}$)—the criterion carries information beyond the calibration-strength trend, chiefly by ordering the method families. Within the 30 conformal configurations alone, after controlling m , assignment, and k , the residual signal is weak ($+0.21$, $p=0.27$): consistent with the region-selector reading, the criterion distinguishes families and calibration regimes, not neighbors within a family.

Table I translates the correlation into the deliverable on

TABLE I
MODEL SELECTION ON DCASE 2025 TASK 2 (EVALUATION SET, OFFICIAL Ω , %; BEATs BACKBONE, 45-CONFIGURATION GRID). ROWS 2–4 SELECT WITH THE LABEL-FREE CRITERION (EQ. (3)); ROW 1 USES LABELED DEV DATA (STANDARD PRACTICE). “ \pm ” IS THE STANDARD DEVIATION OVER TEN CRITERION SEEDS (POOL OF SEVEN $k=1$ SOFT CONFIGURATIONS FROM THE 45-GRID; THE NINE-CONFIGURATION 51-GRID POOL OF TABLE II GIVES 59.63). EVALUATION GROUND TRUTH ENTERS METRIC COMPUTATION ONLY. OFFICIAL-EVALUATOR-VERIFIED.

Selection rule	Chosen configuration	Eval Ω
dev Ω (standard)	raw kNN ($k=1$)	55.83
criterion on dev machines	conf. soft $m=0$, $k=1$	59.34
criterion on eval train normals	conf. soft $m=0$, $k=2$	59.27
per-machine blind (10 seeds)	mixed	59.14 ± 0.12
oracle best fixed config	conf. hard $m=0$, $k=2$	59.55

this grid. Selecting the configuration that minimizes the criterion on the dev machines—selection that uses no evaluation-machine data at all—and deploying it unchanged yields $\Omega = 59.34$ vs. 55.83 for the best-dev- Ω configuration: $+3.5$ points from changing only the selection yardstick (machine-level jackknife 95% CI $[2.2, 4.8]$, leave-one-machine-out range $[3.2, 4.0]$; paired clip-level stratified bootstrap $[2.5, 4.7]$), within 0.21 of the best fixed configuration in hindsight. The two smallest criterion values differ by 0.004—inside seed noise—so the pick can flip to conf. hard $m=0$, $k=1$ (59.50); all plausible picks lie in 59.3–59.6. Per-machine blind selection over a fixed nine-configuration pool (the $k=1$ soft-assignment representatives: raw, the five conformal strengths, median-ratio, LDN-ratio $K=1$, and calibration-on-LDN) attains 59.14 ± 0.12 over ten criterion seeds (min 58.91). Within the top cluster the criterion’s ranking is at chance—it is a region selector, and the whole low-criterion region is good.

For context on the absolute scale: the official evaluation-set baselines score 56.51 (Selective Mahalanobis) and 54.43 (Simple AE), and the top three of 35 teams scored 61.63, 61.57, 61.20 [1]. The dev-selected raw system (55.83) falls below the stronger official baseline—rank 23 among teams—despite beating both baselines on dev (section VI-A): dev-based selection does not merely lose points, it publishes a system worse than the baseline. Criterion-based selection turns the identical pool into rank 7 (59.34), and with the E5 family into rank 4 (61.05, section VI-D)—as a single training-free system with no ensembling, no fine-tuning, and post-challenge timing.

D. Robustness across backbones (E4)

Table II repeats the study on the extended 51-configuration grid for three frozen backbones. The criterion (computed on dev machines) remains a reliable rank predictor on every backbone ($\rho_s +0.81/+0.80/+0.67$), whereas dev Ω swings from useless (-0.03 , BEATs; $+0.11$, EAT) to strong ($+0.84$, PANNs): with PANNs embeddings, dev and evaluation machines happen to agree, so standard selection works there—but one cannot know in advance which regime a given system is in, and only the criterion is reliable in both. Guarded selection (bottom-decile veto + criterion) gains $+5.2$ (BEATs) and $+2.3$ (EAT) points over dev- Ω selection and costs -1.2

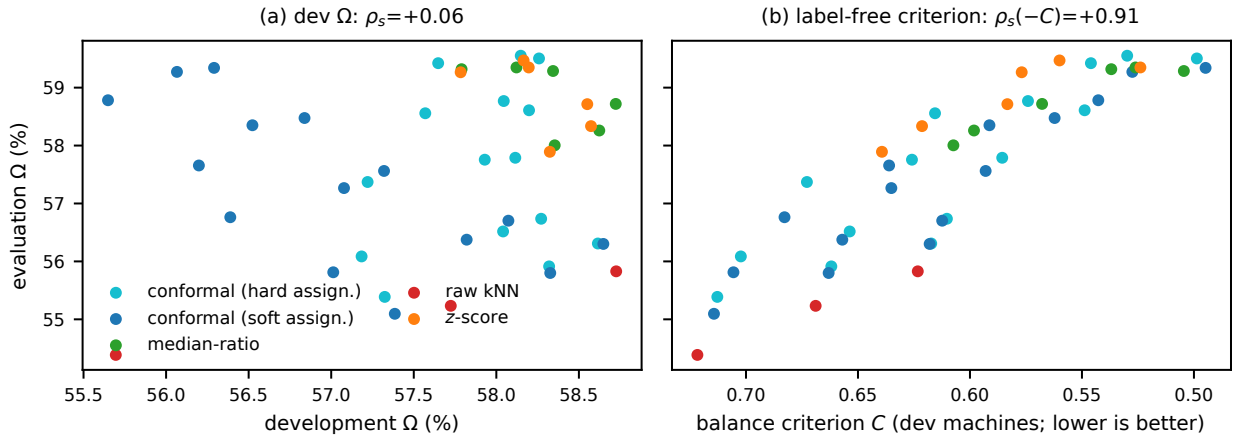


Fig. 3. What predicts evaluation-set performance? Each point is one of 45 configurations (BEATs backbone); colors denote the five method groups (the soft and hard variants of median-ratio and z -score share their group’s color, so the seven families map to five colors). (a) Dev Ω is uninformative—the standard selection signal fails. (b) The label-free CV domain-balance criterion C (eq. (3), computed on dev machines; axis reversed so better is rightward) rank-predicts evaluation Ω .

on PANNs, where dev selection is coincidentally oracle-optimal; the mean gain is $+2.1$. Table II also situates selection against reference rules: a uniformly random configuration averages 54.8–57.8, and the fixed a-priori default (full equalization, conf. soft $m=0$, $k=1$) is itself a strong label-free rule (59.34/58.87/55.55)—guarded selection beats it only on BEATs ($+1.7$, where it finds the LDN stack) and ties it elsewhere, so the criterion’s marginal value over a sensible fixed default is concentrated where the grid contains a genuinely better family. The unguarded criterion-only row makes the veto’s contribution explicit (45.26 on EAT without it). On the grid itself, soft vs. hard assignment and $k \in \{1, 2, 4\}$ shift results by well under a point; the calibration variant matters less than the strength m .

Veto disclosure. The veto was introduced *after* observing that criterion-only selection picks a degenerate configuration on EAT (section VI-E); it is not a pre-registered rule, and we report it transparently. The threshold form (δ from dev-best) selects identically for $\delta \in [3, 8]$ on BEATs and PANNs; on EAT, $\delta \leq 5$ also excludes the three best evaluation configurations (the LDN family, whose dev deficit is ≈ 5.5 points there), costing 0.9 points against the veto-free oracle, while $\delta=8$ recovers them (59.75). The rank-based bottom-decile form used in table II makes the same picks as $\delta=5$ on all three backbones. The residual meta-selection risk (choosing the veto form) is bounded by this spread (58.87–59.75 on EAT) and is disclosed rather than optimized away.

E. Comparison with local-density normalization (E5)

Table III compares against our reimplementations of local-density normalization (LDN) [13], [3] on identical embeddings; all LDN statements in this paper concern this reimplementations from the published equations, not the authors’ system (which couples the normalization to trained embeddings). The density neighborhoods $K \in \{1, 16\}$ cover both papers’ recommendations: $K=1$ for the official metric [3] and $K=16$ from the ICASSP study [13]. Three observations.

TABLE II
SELECTION ACROSS FROZEN BACKBONES (EVALUATION-SET OFFICIAL Ω , %; 51 CONFIGURATIONS PER BACKBONE). “GUARDED CRITERION” = BOTTOM-DECILE DEV- Ω VETO + CRITERION MINIMUM (ALGORITHM 1). REFERENCE ROWS: EXPECTED SCORE OF A UNIFORMLY RANDOM CONFIGURATION (MEAN \pm SD OVER THE 51 CONFIGURATIONS), THE FIXED A-PRIORI DEFAULT (FULL EQUALIZATION: CONF. SOFT $m=0$, $k=1$; DESIGNATED BEFORE THE E7 REPLICATION), AND THE UNGUARDED CRITERION MINIMUM. BEST NON-ORACLE RULE PER BACKBONE IN BOLD.

	BEATs	EAT	PANNs
random configuration	57.8 \pm 2.1	57.5 \pm 2.1	54.8 \pm 1.5
raw kNN ($k=1$)	55.83	56.59	54.23
fixed default (conf. soft $m=0$)	59.34	58.87	55.55
selected by dev Ω	55.83	56.59	56.83
criterion only (no veto)	61.05	45.26	55.58
selected by guarded criterion	61.05	58.87	55.58
per-machine blind (fixed pool)	59.63	60.38	56.66
oracle best fixed config	61.05	59.76	56.83
$\rho_s(\text{dev } \Omega, \text{eval } \Omega)$	-0.03	+0.11	+0.84
$\rho_s(-\text{criterion}, \text{eval } \Omega)$	+0.81	+0.80	+0.67

First, LDN is strong on the evaluation set (ratio variant: 61.04 for both K ; the agreement is coincidental at two decimals, 61.039 vs. 61.040—the density is computed over the full 1000-clip bank, so $K=16$ is well-defined despite the 10-clip target subset)—but *weaker than raw on the dev set* (56.5/57.2 vs. 58.7), so dev-based selection would reject it: even a strong normalization method is a victim of the selection trap this paper addresses, and the criterion selects into its family. Second, calibration stacked on LDN scores (61.05) is statistically indistinguishable from LDN alone (61.04; the margin is far inside seed noise)—the value of the stack is that it is what the guarded criterion picks, not that composition adds points. Third, the difference variant with a large density neighborhood (diff, $K=16$) collapses to a degenerate, well-balanced but non-detecting score map (44.8–49.7 evaluation Ω across backbones). This is expected by construction—subtracting a large summed-distance density term drowns the query distance—and is consistent with the original authors’

TABLE III

DACO VS. LOCAL-DENSITY NORMALIZATION ON IDENTICAL BEATS EMBEDDINGS (OFFICIAL Ω , %). LDN REIMPLEMENTED FROM THE EQUATIONS OF [13], [3]. THE DEV/EVAL AGREEMENT IN THE MEDIAN-RATIO ROW IS COINCIDENTAL (58.7233/58.7189).

System	Dev Ω	Eval Ω
raw kNN ($k=1$)	58.73	55.83
LDN ratio, $K=1$	56.47	61.04
LDN ratio, $K=16$	57.24	61.04
LDN difference, $K=1$	57.94	60.23
LDN difference, $K=16$ (degenerate)	50.39	49.68
per-domain z -score (soft, $k=1$)	58.55	58.71
per-domain median-ratio (soft, $k=1$)	58.72	58.72
DACO (conf. soft $m=0$, $k=1$)	56.29	59.34
DACO on LDN-ratio $K=1$	56.56	61.05

report that, under the official metric, “performance drops rapidly when increasing the value of K ” [3] (the difference variant itself is published only at $K=1$, so $K=16$ -difference is unanchored in prior work); it is exactly the class of configuration a balance-only criterion cannot reject. Criterion-only selection falls for it in three of the five year-backbone settings where the family is present—both replication years and the EAT backbone in 2025 (tables II and IV)—the concrete failure that motivates the viability veto.

Reimplementation validation. The journal version of [3] reports frozen-BEATs LDN results on DCASE 2023 and 2024 under the official metric, which our replication years cover with the same datasets: their raw-kNN baselines (59.0 and 58.2 evaluation Ω) are within 1.1 points of ours (57.95, 57.64), and the qualitative pattern of their $K=1$ gains—evaluation-set gains much larger than dev-set gains, 2023 gains larger than 2024—reproduces in our reimplementation (e.g., ratio $K=1$ on evaluation: +4.6/+1.5 vs. their +8.6/+4.2). Absolute deltas are roughly halved, consistent with the different embedding readout (they use a 6144-d flattened patch embedding scored with MSE; we use the 768-d temporal mean with cosine distance); exact reproduction is not possible from the papers alone, and all LDN rows here should be read as our reimplementation under our readout.

F. Replication across challenge years and a pre-registered forward test (E7)

The 2025 study is one dev→eval machine-set pair. We replicated the complete pipeline—identical 51-configuration grid, criterion, veto, and BEATs backbone—on DCASE 2023 (7 evaluation machine types) and DCASE 2024 (9 types), scoring with the respective official post-challenge ground truth. Table IV shows the result. Two findings replicate without qualification: dev Ω carries no rank information about evaluation Ω in *any* year ($\rho_s=+0.18/+0.13/-0.03$, all n.s. under every treatment we applied); and the degenerate LDN-diff- $K=16$ trap is selected by the unguarded criterion in both replication years (47.6/47.5)—and on the EAT backbone in 2025 (table II)—that is, in three of the five year-backbone settings containing the family, so the veto is not a 2025 artifact, and the guarded rule never selects a broken configuration.

The criterion’s predictive power requires more care. Raw full-grid correlations are +0.54 (2023), −0.10 (2024), +0.81

TABLE IV

REPLICATION ACROSS CHALLENGE YEARS (BEATS, 51 CONFIGURATIONS, EVALUATION-SET OFFICIAL Ω , %). CORRELATION SIGNIFICANCE IS ASSESSED BY FAMILY-BLOCK BOOTSTRAP (TEN FAMILIES, 5000 DRAWS); “N.S.” = THE 95% CI CROSSES ZERO. \dagger NAIVE PER-CONFIGURATION $p<10^{-4}$, BUT THE FAMILY-BLOCK CI $[-0.09, +0.70]$ CROSSES ZERO AND THE FAMILY-MEAN PERMUTATION $p=0.23$; SEE SECTION VI-F. PER-MACHINE BLIND USES THE NINE-CONFIGURATION POOL OF TABLE II, CRITERION SEED 0. BEST LABEL-FREE RULE PER YEAR IN BOLD.

	2023	2024	2025
$\rho_s(\text{dev } \Omega, \text{eval } \Omega)$	+0.18 n.s.	+0.13 n.s.	−0.03 n.s.
$\rho_s(-\text{criterion}, \text{eval } \Omega)$	+0.54 \dagger	−0.10 n.s.	+0.81
raw kNN ($k=1$)	57.95	57.64	55.83
selected by dev Ω	62.23	57.64	55.83
criterion only (no veto)	47.60	47.48	61.05
selected by guarded criterion	63.52	56.29	61.05
fixed default (conf. soft $m=0$)	63.68	57.69	59.34
per-machine blind (fixed pool)	63.38	57.63	59.63
oracle best fixed config	64.14	60.11	61.05

(2025), but the naive per-configuration p -values overstate evidence because configurations cluster into families: under the same family-block apparatus used in section VI-C (block bootstrap over the ten families of the 51-grid; Monte-Carlo permutation of family means, 200k draws), only 2025 survives—CI [+0.43, +0.93] excluding zero—while the 2023 CI crosses zero ($[-0.09, +0.70]$); family-mean permutation $p=0.23$ and, after partialling out family membership and $\log m$, the residual 2023 association is in fact *negative* (−0.61). We therefore claim demonstrated criterion transfer in *one year of three* and read 2023 as family-composition-driven. Selection deltas tell the same story (machine-level jackknife CIs): guarded selection beats dev- Ω selection significantly only in 2025 (+5.2, [1.3, 9.2]; 2023 +1.3 [−1.2, +3.8]; 2024 −1.4 [−4.0, +1.3]), and its differences against the fixed full-equalization default are within machine-level noise in all three years (−0.2 [−1.7, +1.4]; −1.4 [−3.0, +0.2]; +1.7 [−1.2, +4.6]). The fixed default (conf. soft $m=0$, $k=1$)—designated *before* the replication was run, as the E3 criterion pick and the frontier’s full-equalization endpoint—matches or beats guarded selection in both replication years and is the honest recommendation when nothing is known about the target year; per-machine blind selection tracks it closely (63.38/57.63/59.63, table IV), as its per-machine choices are dominated by $m=0$ variants. The criterion’s demonstrated added value is concentrated in 2025, where the configuration space contains family-level structure worth finding (the LDN stack); the veto’s value — catching degenerate configurations — replicates in every year where the degenerate family is present.

Frozen forward test on DCASE 2026. DCASE 2026 retains the source/target single-threshold protocol with two-channel, noise-focused recordings [35]. Its timeline at the time of writing: the evaluation audio was published on 2026-06-01 (Zenodo record 20437238), challenge submissions closed on 2026-06-15, and the team leaderboard was announced on 2026-06-30 (175 submissions; top official score 70.24; official MSE baseline 59.80)—but the *per-clip evaluation ground truth* that

TABLE V
EFFICIENCY (SINGLE RTX 4070 Ti SUPER; 10-S CLIPS AT 16 KHZ,
BATCH 8).

Backbone	Params (M)	Dim	ms/clip	VRAM (MB)
BEATs	90.3	768	9.4	824
EAT-base	90.0	768	7.2	621
PANNs CNN14	81.0	2048	1.9	703

offline scoring requires has not been released. We ran the full selection on the released 2026 *development* set and froze the outcome in the public repository (PREREGISTRATION.md: selected configuration per channel policy, veto rule, criterion seeds, and SHA-256 hashes of the selection artifacts) on 2026-07-03—after the evaluation audio and leaderboard were public, but before the per-clip ground truth became available—so the frozen configuration could not have been evaluated, directly or indirectly, at freezing time. The primary frozen pick (channel 0 policy) is the per-domain median-ratio configuration with hard assignment ($k=2$)—notably *not* the fixed default, making the test discriminative. We commit to scoring the frozen pick, the dev- Ω pick, and the fixed default with the official evaluator as soon as the ground truth is published, and to reporting the outcome in this section whatever it is.

G. Computational cost (E6)

All results were produced on one consumer GPU (RTX 4070 Ti SUPER, 16 GB). Embedding extraction dominates and runs once (table V); on cached embeddings a full per-machine configuration cycle (base scores, LOO, calibration, and the 10-split criterion) takes ~ 0.15 s on CPU, so the complete 51-configuration \times 15-machine study runs in under four minutes per backbone. Peak extraction VRAM is below 1 GB.

VII. DISCUSSION AND LIMITATIONS

a) Why does the criterion transfer while dev Ω does not?:

The criterion measures how well a configuration equalizes the two domains’ normal-score distributions—a property of the *operating point*, not of any machine’s anomaly geometry. The evaluation machines reward balance (raw target AUCs as low as 33.7 on *CoffeeGrinder*; per-machine table in the Appendix); several dev machines punish it (section VI-B). A signal tied to threshold placement rather than to dev-set anomaly idiosyncrasies tracks the quantity that generalizes.

b) *Scope of the transfer evidence*: On dev machines the criterion does *not* predict dev Ω ($\rho_s=+0.16$); blind selection there would have cost 2.7 points. Our claim is not that the criterion predicts any set’s performance, but that it predicts *evaluation* performance where dev Ω does not—and the three-year replication (section VI-F) bounds this claim honestly. What replicates without exception across 2023/2024/2025 and across three backbones: dev Ω is never a *reliable* selection signal—it swings from useless to coincidentally optimal (PANNs; the 2023 dev pick gained +4.3 over raw) and one cannot know in advance which regime applies—and a well-balanced degenerate configuration always exists in the

pool (the unguarded criterion selects it in three of five year-backbone settings). What is year-dependent: the criterion’s predictive power (+0.54, -0.10 , +0.81 raw; only 2025 robust to family clustering), which tracks how much family-level structure the configuration space contains and how much headroom the year offers (the 2024 oracle is only 2.5 points above raw). A practitioner cannot tell the regimes apart in advance; the defensible default is therefore the fixed full-equalization configuration, with criterion-based selection as the no-worse-than upgrade whenever a heterogeneous configuration pool is on the table. The added noise axis of DCASE 2026 is itself a new confound for the criterion—the pre-registered forward test (section VI-F) will answer it prospectively.

c) *Balance is necessary, not sufficient*: A label-free criterion cannot observe detection power, and degenerate score maps achieve excellent balance while detecting nothing (section VI-E). The viability veto closes this with labeled dev data used at the coarse level where they are reliable. This division of labor—dev labels veto broken configurations, the label-free criterion ranks the viable ones—is, we believe, the right general template for model selection under the first-shot protocol; its residual meta-choices are quantified in section VI-D.

d) *Granularity and validity of ten-clip calibration*: With $n_t=10$ the quantile map has data support only down to exceedance $1/11 \approx 0.091$; nearly all of the pAUC range is extrapolated, and pAUC additionally pools domains, so the support boundary maps onto the metric only loosely. Empirically the maps *undercover* under train \rightarrow test session shift: the realized false-positive rate exceeds the nominal level (≈ 0.21 at nominal 0.10, section VI-B), i.e., the calibrated threshold is anti-conservative in absolute terms even where cross-domain balance improves. The weighted-conformal small- n analysis of [21] and group-conditional constructions [18] suggest principled refinements.

e) *Criterion scale across families*: The criterion’s absolute value is not perfectly comparable across method families (hard-assignment configurations outperform soft ones by up to ≈ 2.3 Ω points at closely matched criterion values ($|\Delta C| < 0.005$); within-family it is reliable. Cross-family selection should therefore be read as region-selection, consistent with the 0.21-point oracle gap on the E3 grid (the gaps are 0.9 and 1.25 on EAT and PANNs, table II).

f) *Threats to validity*: (i) Post-challenge ground truth could leak through experimenter iteration; selection signals are computed from training normals (plus dev labels for the veto), the pipeline was audited for leakage, and headline numbers were reproduced by the official evaluator on exported scores. (ii) The evaluation set is scored offline; the evaluator is the official one. (iii) Criterion seeds shift composed selection by ± 0.12 Ω ; fixed-configuration picks can flip within the 59.3–59.6 cluster. (iv) The veto was introduced after observing a failure case and its meta-choices are disclosed, not pre-registered.

VIII. CONCLUSION

We reframed the two open problems of first-shot domain-generalized ASD—the source/target trade-off and dev \rightarrow eval

non-transfer—as calibration and model-selection problems. A per-domain quantile-calibration layer with a shrinkage knob makes calibration strength selectable; a label-free cross-validated balance criterion, paired with a coarse dev-side viability veto, selects the operating point. Across three challenge years, development score is never a reliable selection signal and well-balanced degenerate configurations always lurk in the pool; the criterion’s demonstrated transfer is concentrated in DCASE 2025, where it lifts a training-free frozen-embedding system from below the official baseline to fourth place among challenge teams at ~ 0.15 s per configuration cycle—while in both replication years a fixed full-equalization default matches or beats criterion-based selection. The method applies unchanged on top of any frozen embedding and training-free backend; the frozen DCASE 2026 forward test, fixed before the per-clip evaluation ground truth became available, will extend the evidence prospectively.

DATA AND CODE AVAILABILITY

The DCASE Task 2 datasets are public on Zenodo: 2025 (records 15097779, 15392814, 15519362), 2023 (7882613, 7830345, 7860847), 2024 (10902294, 11259435, 11363076), and the 2026 development set (19336329); 2023/2024 evaluation ground truth comes from the official `nttcslab/dcasetask202{3,4}_task2_evaluator` repositories, and the pre-registration of the 2026 forward test (frozen configuration, artifact hashes) is `PREREGISTRATION.md` in our repository. The 2025 ground truth is published in the official evaluator repository (`nttcslab/dcasetask2025_task2_evaluator`).

All experiment code, per-machine result CSVs, diagnostic artifacts, and the scripts computing every statistic in this paper (bootstrap CIs, FPR coverage, criterion floor, differential metric test) are available at <https://github.com/polestvr/daco-experiments>. Backbone checkpoints: BEATs iter3+ AS2M, EAT `worstchan/EAT-base_epoch30_pretrain` (both MIT), PANNs `Cnn14_16k_mAP=0.438` (Zenodo record 3987831, CC-BY). The local-density-normalization comparison is a clean-room reimplementation from the published equations; the AGPL-licensed reference implementation was not consulted.

APPENDIX

PER-MACHINE RESULTS

Table VI reports per-machine metrics (BEATs backbone) for the dev-selected system (raw kNN), the E3 criterion pick (conf. soft $m=0$, $k=1$), and the guarded pick (DACO on LDN-ratio $K=1$).

TABLE VI
 PER-MACHINE RESULTS (BEATS; %). FOR EACH SYSTEM: AUC_s / AUC_t / pAUC.

Machine	raw kNN ($k=1$)			conf. soft $m=0, k=1$			DACo on LDN ($K=1$)		
	AUC _s	AUC _t	pAUC	AUC _s	AUC _t	pAUC	AUC _s	AUC _t	pAUC
<i>development machines</i>									
bearing	60.6	48.0	57.5	60.3	49.1	57.6	67.1	64.2	62.5
fan	61.2	41.2	48.8	52.3	49.7	48.4	43.4	57.0	52.3
gearbox	65.5	51.2	55.0	61.2	53.9	55.0	63.4	58.0	54.6
slider	75.4	52.9	51.2	74.6	54.4	51.4	72.5	48.7	55.3
ToyCar	75.8	59.0	52.1	35.2	84.5	48.4	32.6	83.3	50.7
ToyTrain	85.0	69.8	53.8	65.0	61.4	52.4	67.7	63.8	49.8
valve	72.3	76.7	61.5	72.9	76.7	61.7	66.6	63.4	56.7
<i>evaluation machines</i>									
AutoTrash	79.6	48.7	50.8	72.1	66.2	50.8	77.1	69.2	56.8
BandSealer	70.3	47.3	55.0	63.8	56.0	56.5	63.2	63.3	59.8
CoffeeGrinder	74.6	33.7	50.1	70.4	41.7	52.3	77.3	43.6	53.4
HomeCamera	74.3	34.8	51.7	69.0	40.9	51.8	65.6	48.0	52.3
Polisher	75.2	40.4	51.7	69.3	52.9	53.0	76.9	52.1	55.2
ScrewFeeder	80.1	88.7	72.0	81.9	90.7	75.3	83.8	94.8	78.0
ToyPet	80.0	47.1	56.6	68.0	63.1	57.9	68.9	72.7	58.7
ToyRCCar	63.4	56.6	52.3	61.0	58.6	52.4	58.8	44.2	51.6
Ω (dev)		58.73			56.29			56.56	
Ω (eval)		55.83			59.34			61.05	

REFERENCES

- [1] T. Nishida, N. Harada, D. Niizumi, D. Albertini, R. Sannino, S. Pradolini, F. Augusti, K. Imoto, K. Dohi, H. Purohit, T. Endo, and Y. Kawaguchi, "Description and discussion on DCASE 2025 challenge task 2: First-shot unsupervised anomalous sound detection for machine condition monitoring," in *Proc. Detection and Classification of Acoustic Scenes and Events Workshop (DCASE)*, 2025, pp. 55–59, official DCASE 2025 Task 2 organizers' paper.
- [2] N. Harada, D. Niizumi, Y. Ohishi, D. Takeuchi, and M. Yasuda, "First-shot anomaly sound detection for machine condition monitoring: A domain generalization baseline," in *Proc. European Signal Processing Conference (EUSIPCO)*, 2023, pp. 191–195.
- [3] K. Wilkinghoff, H. Yang, J. Ebberts, F. G. Germain, G. Wichern, and J. Le Roux, "Local density-based anomaly score normalization for domain generalization," *IEEE Transactions on Audio, Speech and Language Processing*, vol. 33, pp. 4642–4652, 2025.
- [4] K. Wilkinghoff, "Sub-cluster AdaCos: Learning representations for anomalous sound detection," in *Proc. International Joint Conference on Neural Networks (IJCNN)*, 2021, pp. 1–8.
- [5] —, "Self-supervised learning for anomalous sound detection," in *Proc. IEEE International Conference on Acoustics, Speech and Signal Processing (ICASSP)*, 2024, pp. 276–280.
- [6] —, "AdaProj: Adaptively scaled angular margin subspace projections for anomalous sound detection with auxiliary classification tasks," in *Proc. Detection and Classification of Acoustic Scenes and Events (DCASE) Workshop*, 2024, pp. 186–190.
- [7] K. Wilkinghoff, T. Fujimura, K. Imoto, J. Le Roux, Z.-H. Tan, and T. Toda, "Handling domain shifts for anomalous sound detection: A review of DCASE-related work," in *Proc. Detection and Classification of Acoustic Scenes and Events (DCASE) Workshop*, 2025, pp. 20–24.
- [8] S. Chen, Y. Wu, C. Wang, S. Liu, D. Tompkins, Z. Chen, W. Che, X. Yu, and F. Wei, "BEATS: Audio pre-training with acoustic tokenizers," in *Proc. International Conference on Machine Learning (ICML)*, 2023, pp. 5178–5193.
- [9] W. Chen, Y. Liang, Z. Ma, Z. Zheng, and X. Chen, "EAT: Self-supervised pre-training with efficient audio transformer," in *Proc. International Joint Conference on Artificial Intelligence (IJCAI)*, 2024, pp. 3807–3815.
- [10] Q. Kong, Y. Cao, T. Iqbal, Y. Wang, W. Wang, and M. D. Plumbley, "PANNs: Large-scale pretrained audio neural networks for audio pattern recognition," *IEEE/ACM Transactions on Audio, Speech, and Language Processing*, vol. 28, pp. 2880–2894, 2020.
- [11] P. Saengthong and T. Shinozaki, "Deep generic representations for domain-generalized anomalous sound detection," in *Proc. IEEE International Conference on Acoustics, Speech and Signal Processing (ICASSP)*, 2025.
- [12] J. Zhou and M. Wang, "Scoring backends matter more than pooling: A systematic study of training-free anomalous sound detection under domain shift," 2026.
- [13] K. Wilkinghoff, H. Yang, J. Ebberts, F. G. Germain, G. Wichern, and J. Le Roux, "Keeping the balance: Anomaly score calculation for domain generalization," in *Proc. IEEE International Conference on Acoustics, Speech and Signal Processing (ICASSP)*, 2025, pp. 1–5.
- [14] K. Wilkinghoff, G. Wichern, J. Le Roux, and Z.-H. Tan, "Mind the gap: Detecting cluster exits for robust local density-based score normalization in anomalous sound detection," *arXiv preprint arXiv:2602.18777*, 2026.
- [15] V. Vovk, A. Gammerman, and G. Shafer, *Algorithmic Learning in a Random World*. Springer, 2005.
- [16] R. Laxhammar and G. Falkman, "Inductive conformal anomaly detection for sequential detection of anomalous sub-trajectories," *Annals of Mathematics and Artificial Intelligence*, vol. 74, pp. 67–94, 2015.
- [17] A. N. Angelopoulos and S. Bates, "Conformal prediction: A gentle introduction," *Foundations and Trends in Machine Learning*, vol. 16, no. 4, pp. 494–591, 2023.
- [18] T. Ding, A. N. Angelopoulos, S. Bates, M. I. Jordan, and R. J. Tibshirani, "Class-conditional conformal prediction with many classes," in *Advances in Neural Information Processing Systems (NeurIPS)*, 2023.
- [19] I. Gibbs, J. J. Cherian, and E. J. Candès, "Conformal prediction with conditional guarantees," *Journal of the Royal Statistical Society Series B: Statistical Methodology*, vol. 87, no. 4, pp. 1100–1126, 2025.
- [20] N. Martínez Gil, F. O'Donncha, W. M. Gifford, N. Zhou, D. C. Patel, and R. Vaculin, "Adaptive conformal anomaly detection with time series foundation models for signal monitoring," in *Proc. International Conference on Learning Representations (ICLR)*, 2026.
- [21] O. Hennhöfer and C. Preisach, "Between resolution collapse and variance inflation: Weighted conformal anomaly detection in low-data regimes," 2026.
- [22] S. Yuan, J. Li, C. Wang, and X. Zhang, "Conformal machine learning for reliable anomaly detection in industrial cyber-physical systems," *Reliability Engineering & System Safety*, vol. 274, p. 112417, 2026.
- [23] R. Tibshirani, D. Nevo, and U. Shalit, "Set valued predictions for robust domain generalization," in *Proc. International Conference on Machine Learning (ICML)*, 2025.
- [24] L. Guan, "Localized conformal prediction: a generalized inference framework for conformal prediction," *Biometrika*, vol. 110, no. 1, pp. 33–50, 2023.
- [25] R. Hore and R. F. Barber, "Conformal prediction with local weights: randomization enables robust guarantees," *Journal of the Royal Statistical Society Series B: Statistical Methodology*, vol. 87, no. 2, pp. 549–578, 2025.
- [26] B. Cestnik, "Estimating probabilities: A crucial task in machine learning," in *Proc. 9th European Conference on Artificial Intelligence (ECAI)*, 1990, pp. 147–149.
- [27] A. Gelman and J. Hill, *Data Analysis Using Regression and Multi-level/Hierarchical Models*. Cambridge University Press, 2007.
- [28] Y. Zhao, R. A. Rossi, and L. Akoglu, "Automatic unsupervised outlier model selection," in *Advances in Neural Information Processing Systems (NeurIPS)*, 2021.
- [29] M. Goswami, C. Challu, L. Callot, L. Minorics, and A. Kan, "Unsupervised model selection for time-series anomaly detection," in *Proc. International Conference on Learning Representations (ICLR)*, 2023.
- [30] M. Sugiyama, M. Krauledat, and K.-R. Müller, "Covariate shift adaptation by importance weighted cross validation," *Journal of Machine Learning Research*, vol. 8, no. 35, pp. 985–1005, 2007.
- [31] K. You, X. Wang, M. Long, and M. Jordan, "Towards accurate model selection in deep unsupervised domain adaptation," in *Proc. International Conference on Machine Learning (ICML)*, ser. Proceedings of Machine Learning Research, vol. 97, 2019, pp. 7124–7133.
- [32] K. Saito, D. Kim, P. Teterwak, S. Sclaroff, T. Darrell, and K. Saenko, "Tune it the right way: Unsupervised validation of domain adaptation via soft neighborhood density," in *Proc. IEEE/CVF International Conference on Computer Vision (ICCV)*, 2021, pp. 9164–9173.
- [33] N. Harada, D. Niizumi, D. Takeuchi, Y. Ohishi, M. Yasuda, and S. Saito, "ToyADMOS2: Another dataset of miniature-machine operating sounds for anomalous sound detection under domain shift conditions," in *Proc. Detection and Classification of Acoustic Scenes and Events (DCASE) Workshop*, 2021.
- [34] K. Dohi, T. Nishida, H. Purohit, R. Tanabe, T. Endo, M. Yamamoto, Y. Nikaido, and Y. Kawaguchi, "MIMII DG: Sound dataset for malfunctioning industrial machine investigation and inspection for domain generalization task," in *Proc. Detection and Classification of Acoustic Scenes and Events (DCASE) Workshop*, 2022.
- [35] T. Nishida, N. Harada, D. Takeuchi, D. Niizumi, K. Imoto, K. Dohi, H. Purohit, T. Endo, and Y. Kawaguchi, "Description and discussion on DCASE 2026 challenge task 2: Noise-aware unsupervised anomalous sound detection for machine condition monitoring," 2026.